Resource

Cell Reports

# iTAG-RNA Isolates Cell-Specific Transcriptional Responses to Environmental Stimuli and Identifies an RNA-Based Endocrine Axis

## Graphical Abstract

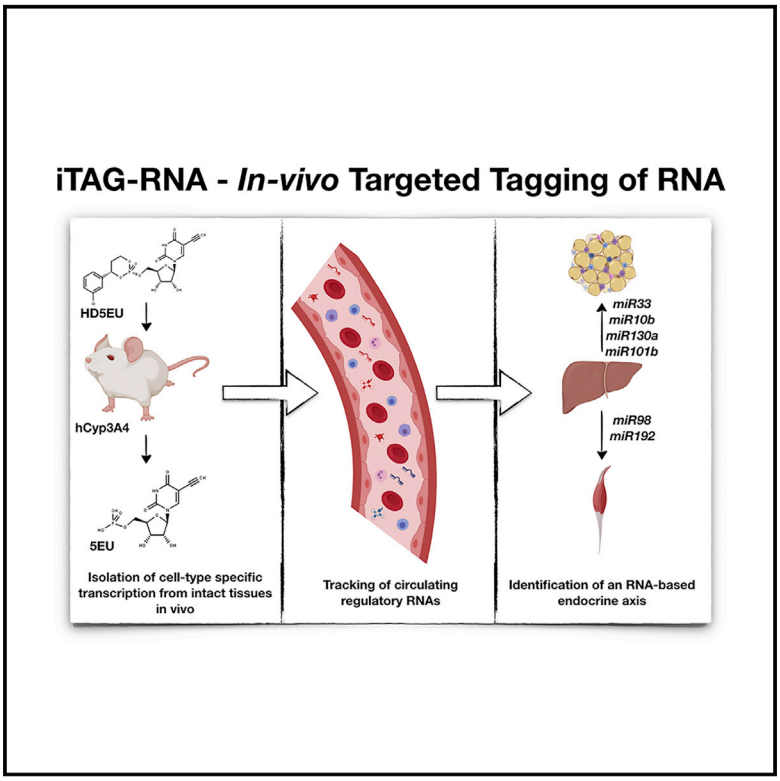


## Authors

Jonatan Darr, Archana Tomar, Maximilian Lassi, ..., Martin Hrabě de Angelis, Michael Witting, Raffaele Teperino

## Correspondence

michael.witting@helmholtz-muenchen.de (M.W.), raffaele.teperino@helmholtz-muenchen.de (R.T.)

## In Brief

RNAs populate biofluids and are potential biomarkers. Their physiological function is not completely understood due to a lack of technologies allowing unbiased transcriptional labeling and source-to-sink RNA tracking. Darr et al. develop iTAG-RNA for unbiased tagging of RNA *in vivo* and identify a diet-sensitive liver-to-adipose and muscle endocrine axis.

## Highlights

- iTAG-RNA allows unbiased *in vivo* targeted tagging of RNA
- iTAG-RNA isolates cell-type-specific responses to diet from an intact tissue *in vivo*
- iTAG-RNA identifies hepatocyte-secreted circulating cell-free RNAs
- iTAG-RNA identifies RNA transfer from liver to adipose tissue and skeletal muscle

Darr et al., 2020, Cell Reports *30*, 3183–3194
March 3, 2020 
https://doi.org/10.1016/j.celrep.2020.02.020

CellPress

Cell Reports
Resource



# iTAG-RNA Isolates Cell-Specific Transcriptional Responses to Environmental Stimuli and Identifies an RNA-Based Endocrine Axis

Jonatan Darr,[1,2] Archana Tomar,[1,2] Maximilian Lassi,[1,2] Raffaele Gerlini,[1,2] Lucia Berti,[2,6] Annette Hering,[1] Fabienne Scheid,[1,2] Martin Hrabě de Angelis,[1,2,3] Michael Witting,[4,5,*] and Raffaele Teperino[1,2,7,*]

[1]Institute of Experimental Genetics, Helmholtz Zentrum München, German Research Center for Environmental Health, Neuherberg, Germany
[2]German Center for Diabetes Research (DZD), Neuherberg, Germany
[3]Experimental Genetics, Faculty of Life and Food Sciences Weihenstephan, Technische Universität München, Freising-Weihenstephan, Germany
[4]Research Unit Analytical BioGeoChemistry, Helmholtz Zentrum München, Oberschleißheim, Germany
[5]Chair of Analytical Food Chemistry, Technische Universität München, Freising, Germany
[6]Institute for Diabetes Research and Metabolic Diseases of the Helmholtz Center Munich at the Eberhard-Karls-University of Tübingen, Tübingen, Germany
[7]Lead Contact
*Correspondence: michael.witting@helmholtz-muenchen.de (M.W.), raffaele.teperino@helmholtz-muenchen.de (R.T.)
https://doi.org/10.1016/j.celrep.2020.02.020

## SUMMARY

**Biofluids contain various circulating cell-free RNAs (ccfRNAs). The composition of these ccfRNAs varies among biofluids. They constitute tantalizing biomarker candidates for several pathologies and have been demonstrated to be mediators of cellular communication. Little is known about their function in physiological and developmental settings, and most works are limited to *in vitro* studies. Here, we develop iTAG-RNA, a method for the unbiased tagging of RNA transcripts in mice *in vivo*. We use iTAG-RNA to isolate hepatocytes and kidney proximal epithelial cell-specific transcriptional responses to a dietary challenge without interfering with the tissue architecture and to identify multiple hepatocyte-secreted ccfRNAs in plasma. We also identify specific transfer of liver-derived ccfRNAs to adipose tissue and skeletal muscle, where they likely constitute a buffering system to maintain lipid homeostasis under acute high-fat-diet feeding. Our findings directly demonstrate *in vivo* transfer of RNAs between tissues and highlight its implications for endocrine signaling and homeostasis.**

## INTRODUCTION

Little is known about the biological function of circulating cell-free RNAs (ccfRNAs). Associated with exosomes, lipoproteins, ribonucleoproteins, and more, ccfRNAs can be isolated and sequenced from multiple biofluids such as plasma, lymph, cerebral fluids, and breast milk (Murillo et al., 2019; Yeri et al., 2017). ccfRNAs are directly implicated in the development of several pathologies, including cancer and obesity (Dror et al., 2016; Castaño et al., 2018; Wortzel et al., 2019), and are intensively studied as disease biomarkers (Schwarzenbach et al., 2014; Gilad et al., 2008). Despite this, their role in physiological and developmental settings and in mediating cell-to-cell communication remains largely unknown. Although a growing number of studies demonstrate the relevance of RNA-based cellular communication *in vitro* (Pegtel et al., 2010; Vickers et al., 2011; Pastuzyn et al., 2018; Kosaka et al., 2010), *in vivo* evidence is still limited. This discrepancy partly arises from the difficulties posed to tracking ccfRNAs from their transcriptional source to the potential sites of action *in vivo*, with limited tools available and few studies attempting to tackle the problem directly.

One work suggested that most circulating microRNAs (miRNAs) originate in adipose tissue and that some adipose-derived miRNAs play a role in the regulation of liver Fgf21 levels (Thomou et al., 2017). However, this work focuses on miRNAs and does not directly demonstrate transfer of RNAs between tissues or directly identify adipose-secreted RNAs.

Transfer of miRNAs was also demonstrated between epithelial cells of the caput epididymis to maturing spermatozoa, leading to a shift in sperm RNA content during its maturation (Sharma et al., 2018). This study used 4-thiouracil tagging (TU tagging) (Gay et al., 2013) combined with SLAM-seq (Herzog et al., 2017) to demonstrate loading of miRNAs transcribed in caput epididymis into maturing spermatozoa. TU tagging entails cell-type-specific expression of uracil phosphoribosyltransferase (UPRT) and administration of 4-thiouracil, with the assumption that only cells expressing UPRT would incorporate 4-thiouracil into transcribing RNA. Thio-RNA can then be purified and used for downstream gene expression analyses or combined with SLAM-seq to identify labeled transcripts. TU tagging has proved useful in several additional systems (Chatzi et al., 2016; Gay et al., 2013; Miller et al., 2009); however, given endogenous (Ghosh et al., 2015) and alternative (Maquat and Kiledjian, 2008) pathways for uracil incorporation, the labeling specificity in this method remains unclear. In addition, as demonstrated

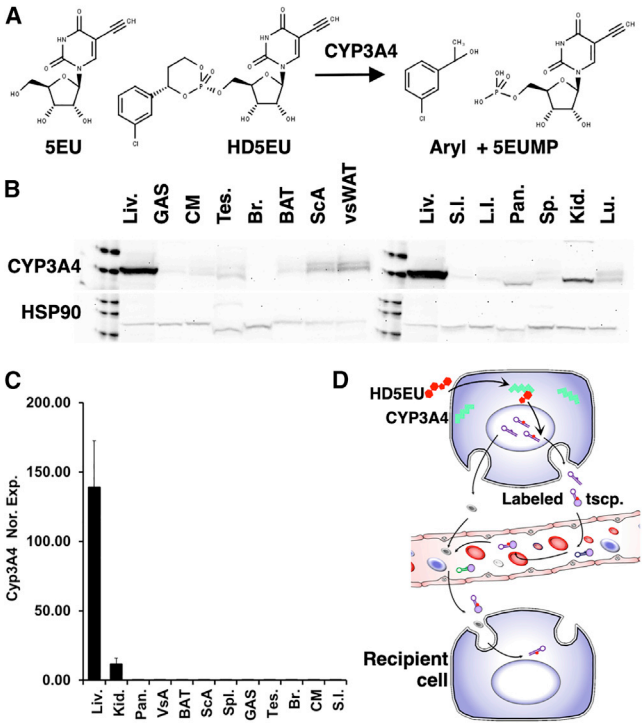


**Figure 1. HD5EU Small-Molecule Design and CYP3A4 Expression Pattern**

(A) HD5EU small molecule and metabolite structure relative to 5EU.

(B) Western blot depicting the tissue expression pattern of CYP3A4 in hCYP3A4 mice. Heat shock protein 90 (HSP90) serves as loading control. GAS, gastrocnemius muscle; CM, cardiac muscle; BAT, brown adipose tissue; ScA, subcutaneous white adipose tissue; vsWAT, visceral white adipose tissue; SI, small intestine; LI, large intestine.

(C) qRT-PCR validating liver- and kidney-specific expression of CYP3A4 (mean ± SD, n = 3).

(D) Administration of the HD5EU small molecule to cells expressing CYP3A4 allows its metabolism into 5EU and subsequent labeling of total RNA. Labeled and secreted transcripts can be identified in biofluids and recipient cells.

by Herzog et al. (2017) and by Sharma et al. (2018), TU tagging of RNA polymerase I (RNA Pol I) and RNA polymerase III (RNA Pol III) transcripts is inefficient, leaving tRNAs and ribosomal transcripts unlabeled.

Only a handful of techniques enable *in vivo* targeted labeling of RNAs. In addition to TU tagging, 5-ethynylcytosine tagging (EC tagging) (Hida et al., 2017) is a new method that uses cell-type-specific co-expression of cytosine deaminase (CD) with UPRT to achieve RNA labeling with 5-ethynyluridine (5EU) following administration of 5-ethynylcytosine. Both TU tagging and EC tagging use Cre recombination to express the relevant enzymes in a tissue-specific manner, and stochastic expression from the Cre promoter may lead to unwanted expression of the enzymes in different tissues (Song and Palmiter, 2018). Finally, one recently developed method called Mime-seq allows for cell-type-specific labeling of miRNAs (Alberti et al., 2018). In this method, tissue-specific expression of a plant-derived methyltransferase mediates a 3′-terminal 2′-O-methylation of miRNAs that when combined with methylation-dependent library construction, allows for sequencing of tissue-specific miRNAs. Mime-seq allows labeling of miRNAs and leaves other RNA biotypes unlabeled.

Given the need for a method that allows Cre-independent and unbiased labeling of total RNA transcription *in vivo*, we developed *in vivo* targeted tagging of RNA (iTAG-RNA). iTAG-RNA couples mouse genetics with a novel uridine analog and an established RNA labeling chemistry to allow tagging of total RNA in target cells *in vivo*. Using iTAG-RNA, we are able to isolate transcriptional reprogramming of hepatocytes *in vivo* following an acute high-fat-diet (HFD) stress and to enrich for and identify hepatocyte-derived plasma ccfRNAs. We also identify specific transfer of hepatocyte-transcribed RNAs to adipose tissue and skeletal muscle. These liver-derived ccfRNAs include variable coding and non-coding RNAs such as miRNAs, tRNAs, and large intergenic noncoding RNAs (lincRNAs). Among the miRNAs, mir-33, mir-10b, mir-130a, and mir-101b were transferred from liver specifically to adipose tissue, whereas mir-98 and mir-192 were transferred specifically to skeletal muscle. mir-33, mir-10b, mir-101b, and mir-130a target major regulators of cholesterol and lipid homeostasis (Marquart et al., 2010; Rayner et al., 2010) and regulate gene expression in both adipose tissue and skeletal muscle.

Our study introduces iTAG-RNA, an unbiased method that allows labeling, tracking, and quantification of several types of ccfRNAs from their transcriptional source to downstream tissues. We demonstrate RNA-based liver-to-periphery transfer of a myriad of RNA transcripts and their response to an environmental challenge. The continued identification and characterization of RNA-based signaling *in vivo* is imperative for the understanding of developmental, physiological, and pathological processes and can aid in the development of relevant disease biomarkers.

## RESULTS

### Small-Molecule Design and Genetic Approach for Targeted *In Vivo* Labeling of RNA

5EU is a synthetic uridine analog extensively used in RNA turnover studies (Jao and Salic, 2008; Best, 2009; Hagemeijer et al., 2012). The nitrogenous base contains an alkyne group that can be covalently linked to an azide group using a simple copper-mediated reaction called click chemistry (Gierlich et al., 2006; Meyer et al., 2016). 5EU incorporates into transcribing RNA in place of uridine and has little to no biological effects thereafter (Jao and Salic, 2008). Following administration to mice, 5EU is readily taken up by cells with no regard to cell identity, depending to some extent on the administration method and dosage used (Jao and Salic, 2008). Here, we introduce a method for the targeted *in vivo* delivery of 5EU.

To achieve this, we designed a pro-drug of 5EU (HD5EU) that is based on the Hep-Direct pro-drug design (Pradere et al., 2014; Erion et al., 2004) (Figure 1A). This design was developed to target small molecules and nucleotide analogs to the human CYP3A4 enzyme, and several small molecules of this design have been or are under clinical study (Boyer et al., 2006; Erion et al., 2007; Reddy et al., 2008). The human CYP3A4 enzyme catalyzes an oxidative cleavage of the HD5EU small molecule that, following a spontaneous

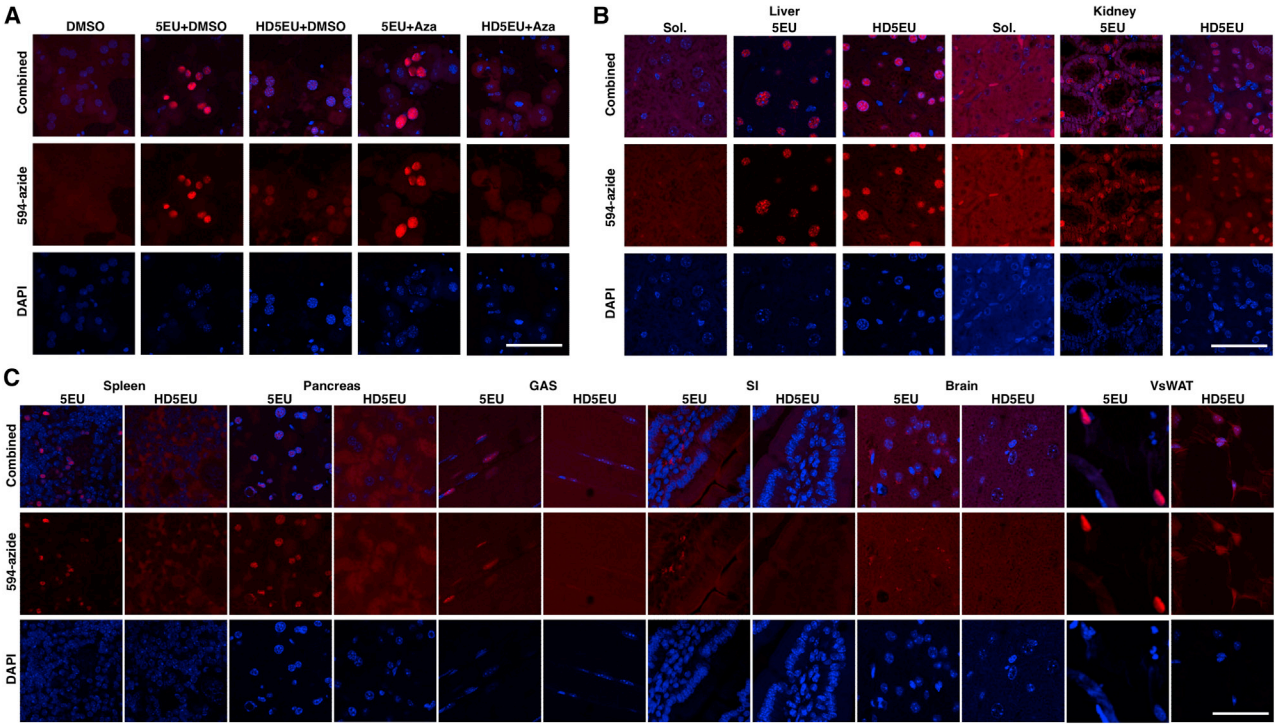


**Figure 2. Tissue-Specific Staining Evident with HD5EU Depends on CYP3A4 Activity**

(A) Staining of 5EU-labeled RNA in primary hepatocytes following treatment with 5EU or HD5EU with or without azamulin pre-treatment. Aza, azamulin; 594-azide, click-it staining.

(B ) Liver- and kidney-specific incorporation of 5EU following 2 h of HD5EU administration to mice.

(C) Tissues with undetectable 5EU incorporation following HD5EU administration. GAS, gastrocnemius muscle; SI, small intestine; VsWAT, visceral white adipose tissue.

Scale bar, 50 μM. For negative controls, see Figure S2.

beta-elimination, results in the formation of 5EU monophosphate, which can then be incorporated into transcribing RNA (Figure 1A). HD5EU was synthesized by Chiroblock; the identity of the final product was validated using mass spectrometry (MS), p-NMR, and h-NMR; and the molecule's purity was assessed as more than 98% (Figure S1).

In addition to the HD5EU small molecule, we took advantage of the published humanized liver-specific CYP3A4 mouse line FVB/129P2-*Cyp3a13*$^{tm1Ahs}$ Del(*5Cyp3a57-Cyp3a59*)$^{1Ahs}$ Tg(*APOE*-CYP3A4)$^{A1Ahs}$ obtained from Taconic (van Herwaarden et al., 2005, 2007). These humanized CYP3A4 (hCYP3A4) mice express the human CYP3A4 enzyme under a modified Apolipoprotein E (APOE) promoter and are stably knocked out for nine homologous murine genes, leaving the human enzyme as the sole member of the family to be expressed in a Cre-independent, tissue-specific manner *in vivo*. In keeping with published data on the activity of the modified ApoE promoter (Simonet et al., 1993), qRT-PCR and western blot (WB) analyses demonstrate restricted expression of the human Cyp3a4 enzyme to liver and kidney (Figures 1B and 1C). As such, upon administration of HD5EU to the hCYP3A4 mice, we expect the molecule to be metabolized to bioavailable 5EU monophosphate exclusively in cells expressing CYP3A4, namely, hepatocytes and kidney proximal renal epithelial cells, thus allowing *in vivo* targeted labeling of transcription and identification of secreted transcripts in biofluids upon pull-down of 5EU-labeled RNA (Figure 1D).

## CYP3A4 Is Necessary for *In Vitro* and *In Vivo* Metabolism of the HD5EU Small Molecule

To test and validate the metabolism of HD5EU, we isolated primary hepatocytes from hCYP3A4 mice. Following an 8-h treatment with 1 mM HD5EU or 5EU, we detected a nuclear signal similar to 5EU labeling by click-it fluorescent staining (Figure 2A). When pre-treated with azamulin, a highly selective CYP3A4 inhibitor (Stresser et al., 2004), nuclear staining was undetectable only in HD5EU-treated cells (Figure 2A). These results indicate that although 5EU is still readily incorporated into transcribing RNA in the nucleus, nuclear staining in HD5EU-treated cells depends on CYP3A4 activity.

We administered HD5EU to hCYP3A4 mice and just 2 h following administration found robust nuclear staining exclusively in hepatocytes and kidney epithelial cells, in contrast to 5EU-treated animals, in which nuclear staining was evident in multiple tissues (Figures 2B and 2C; Figure S2A). Of note, animals administered with HD5EU did not demonstrate visible side effects. In addition, we could not detect signs of DNA damage or apoptosis in the liver during the different treatments , as indicated

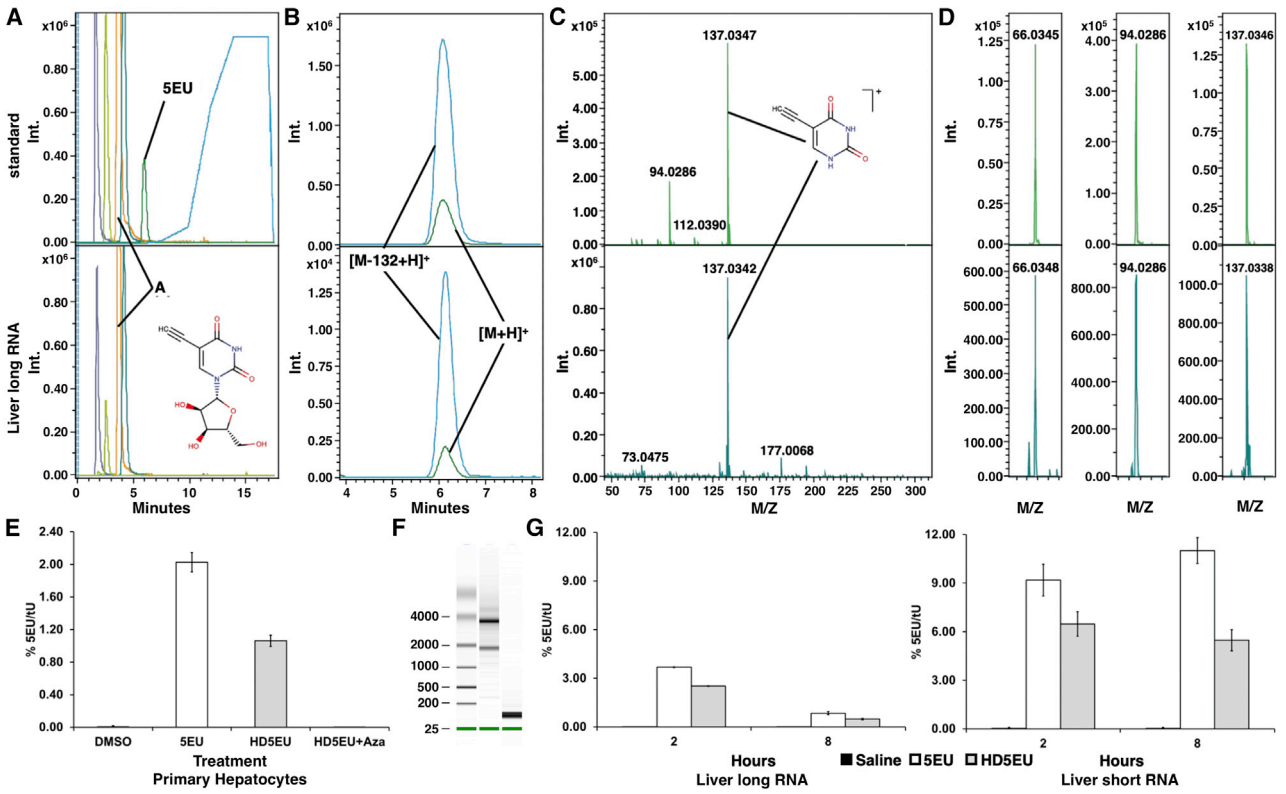


**Figure 3. MS Validation and Quantification of 5EU in Liver RNA of HD5EU-Treated Mice**

(A) Extracted ion chromatograms from the RNA nucleotides A, C, G, and U, as well as 5EU and gradient slope. Int., relative intensity.

(B) Close up of extracted ion chromatograms of 5EU $[M+H]^+$ and the 5EU in-source fragment $[M-132+H]^+$.

(C) Tandem MS spectra at 20 eV of the standard and sample, indicating the main fragment $[M-132+H]^+$.

(D) Further fragments at 40 eV used for identification of 5EU in RNA samples.

(E) Relative quantification of 5EU in primary hepatocytes treated for 8 h with the indicated compounds. Aza, azamulin.

(F) Bioanalyzer image depicting isolation of liver long and short RNA. M, marker; L, long RNA fraction; S, short RNA fraction.

(G) Relative quantification of 5EU in liver-derived long and short RNAs following the indicated time after 5EU or HD5EU administration to mice (mean ± SD, n = 3).

(A–D) Upper panels depict standard nucleotides. Lower panels depict long RNA purified from the liver of HD5EU-treated mice.

by phosph-P53 and cleaved caspase-3 staining, thus supporting HD5EU as a non-toxic agent (Figure S2B).

## Mass-Spectrometric Validation and Quantification of 5EU Incorporation into RNA following HD5EU Treatment

To validate that nuclear staining evident *in vitro* and *in vivo* following HD5EU treatment is indicative of 5EU incorporation into transcribing RNA, we adopted the MS method described by Su et al. (2014). Using a column with a smaller inner diameter and lower flow rates to improve the response of individual nucleotides, we identified a range of unmodified and modified nucleotides (Table S1). 5EU (*m/z* 269.0768) was well separated from the potential interfering 13C-adenosine isotope (adenosine *m/z* 268.1040 and 13C-adenosine *m/z* 269.106541) in standard samples (Figure 3A). Because of the MS settings, all nucleotides show a prominent in-source fragment, which corresponds to the neutral loss of the ribose (denoted as $[M-132+H]^+$) (Figure 3B).

Tandem MS validated that 5EU is present in RNA extracted from the liver of HD5EU-treated mice (Figures 3A–3D). The main fragment at 20-eV collision energy was the neutral loss of $[M-132+H]^+$, consistent with the observed in-source fragment (Figures 3B and 3C). Further fragments of the remaining nucleoside fragment were observed under higher collision energy of 40 eV (Figure 3D). To quantify 5EU incorporation into RNA, we used the prominent in-source fragment of 5EU due to the low abundance of 5EU in biological samples, because this in-source fragment was up to 3- to 5-fold higher than the intact molecule. *In vitro*, azamulin treatment of primary hepatocytes inhibited HD5EU metabolism and incorporation into transcribing RNA (Figure 3E), in line with the observed fluorescent staining (Figure 2A). *In vivo*, we could detect and quantify 5EU incorporation into both short (less than 200 bp) and long RNA isolated from the liver of HD5EU-treated mice 2 h following the administration of the compound (Figures 3F and 3G). 8 h following HD5EU administration, 5EU was still detectable in long RNA (though it could not be accurately quantified, because it was below the quantification limit), whereas only a moderate reduction was detected in short RNA.

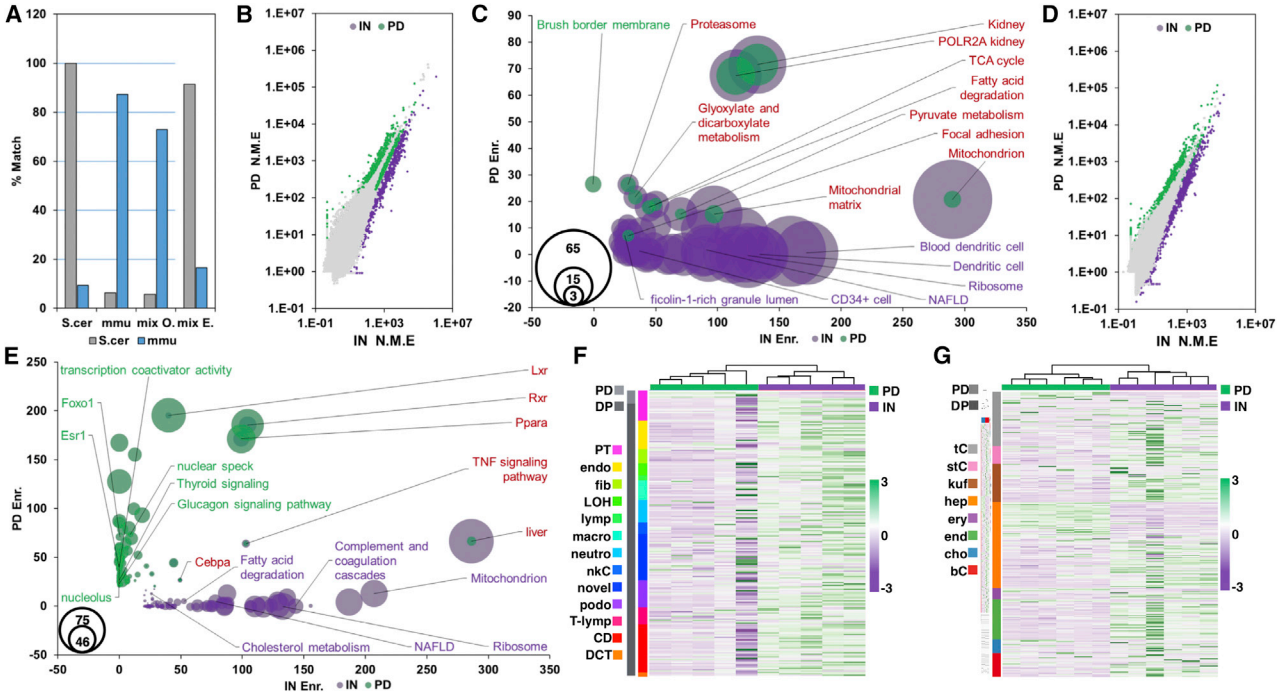


**Figure 4. mRNA Pull-Down Enriches for Specific Cell Populations *In Vivo***

(A) Pull-down of a 10:1 mixture of unlabeled yeast RNA and labeled RNA from mouse liver specifically depletes unlabeled yeast RNA (gray) while enriching labeled mouse RNA (blue). Compare observed (mix O.) ratios of genomic alignment to expected ratios (mix E.).

(B–E) Scatterplot visualizing normalized mean expression (NME) of pull-down (PD, green) versus input (In., purple) poly(A) RNA from mouse kidney (B) or liver (D). Gene Ontology (GO) and gene set enrichment analysis for pull-down (green) versus input (purple) protein-coding transcripts in kidney (C) or liver (E) (bubble size proportional to $-\log_{10}$ of adj. PV).

(F and G) Markers for various cell types from kidney (F) or liver (G) single-cell RNA sequencing (RNA-seq) (Park et al., 2018) and their relative expression in input and pull-down poly(A) RNA libraries.

PT, proximal tubule; endo, endothelial cells; fib, fibroblasts; LOH, loop of Henle; lymp, lymphocytes; macro, macrophages; neutro, neutrophils; nkC, natural killer cells; novel, novel cell type; podo, podocytes; T-lymp, T lymphocytes; CD, collecting duct; DCT, distal convoluted tubule; tC, T cells; stC, stellate cells; kuf, Kupffer cells; hep, hepatocytes; ery, erythrocytes; end, endothelial cells; cho, cholangiocytes; bC, B cells; PD, pull down; DP, depleted; IN, input.

Altogether, these results confirm that HD5EU is metabolized in a CYP3A4-dependent manner to 5EU, which is then incorporated into transcribing RNA *in vivo*.

## Robustness and Reproducibility of RNA Precipitation

2 h following administration of HD5EU, 5EU-containing liver and kidney transcripts can be biotinylated and pulled down for next-generation sequencing. We persistently failed to generate amplified libraries following pull-down of unlabeled RNA isolated from liver, plasma, or kidney of saline-treated control mice (Figures S3A–S3E). In addition, following a 2-h treatment with HD5EU, we generated libraries from modified RNAs pulled down from liver and kidney of treated animals, but we failed to do the same from plasma and additional tissues (Figures S3A–S3E). This result was consistent for both poly(A)-enriched and small RNA libraries and suggests biotinylation to be specific for 5EU-containing transcripts. Technical replicates of pull-down libraries demonstrated a high degree of correlation, supporting the technical robustness and reproducibility of the method (Figure S3F, Spearman correlation coefficient = 0.95).

To further assess the levels of non-specific RNA pull-down, we prepared a 10:1 mixture of non-labeled small RNAs from *S. cerevisiae* and labeled small RNAs derived from mouse liver. Library construction and sequencing of this mixture following RNA pull-down demonstrated highly effective depletion of yeast RNA compared with input (Figure 4A). These results demonstrate RNA pull-down to be highly selective to biotinylated RNA and non-specific RNA precipitation to be extremely low to undetectable.

## RNA Labeling *In Vivo* Uncovers Tissue Architecture and Stress-Induced Transcriptional Reprogramming

We next examined whether *in vivo* labeling enriches for cell-type-specific transcriptional programs within complex tissues *in vivo* and whether we could detect environmentally induced transcriptional reprogramming. To this end, we fed mice with HFD or a control low-fat diet (LFD) for two weeks. Following this acute HFD exposure, which is expected to alter the liver transcriptional program (Williams et al., 2014), we administered HD5EU 2 h before sacrificing and generated poly(A)-enriched libraries from kidney and liver input and pull-down RNA.

Following mapping with the STAR aligner (Dobin et al., 2013), transcript quantification using HTSeq-count, and differential pull-down analyses using the NOISeq package (Tarazona

et al., 2015), we defined pull-down transcripts as those whose abundance can be estimated with a high degree of confidence to be at least half of the abundance observed in input (i.e., at least 50% of the gene's transcripts are labeled with a probability cutoff of 0.975) (Figures 4B–4G; Table S2).

In kidney, in which proximal renal epithelial cells are labeled, Gene Ontology and gene set enrichment analysis using *Enrichr* (Chen et al., 2013) demonstrated enrichment for genes coding for proteins localized to the brush boarder membrane, along with a few more general terms found enriched in input, such as mitochondria, focal adhesion, and genes specific to or highly expressed in the kidney (Figures 4B and 4C; Table S2). The brush boarder membrane is a unique feature of proximal renal epithelial cells (Coudrier et al., 1988), and among pull-down transcripts, Solute Carrier Family 9 member A3 (Slc9a3) is one of its specific markers. Slc9a3 is the sodium-hydrogen antiporter 3 that is highly expressed in the proximal tubule and allows active transport of sodium to the cell. Annotated terms uniquely enriched in genes depleted following pull-down include ribosomal genes and genes highly expressed in CD34-positive or immune cells. CD34-positive cells are likely endothelial cells found in glomeruli and blood vessels in both humans and mice but, importantly, absent from tubules (Lin et al., 1995; Fina et al., 1990).

In liver, enrichment for identified liver targets of the nuclear receptors PPARA, LXR, and RXR is evident in both depleted and pull-down transcripts. Pull-down transcripts demonstrate additional enrichment for identified liver targets of transcription factors such as Foxo1, Clock, and Nucks1 and for transcripts localizing to nuclear speckles and nucleoli (Figures 4D and 4E; Table S2). LXR and RXR are implicated in lipid metabolism and heterodimerize to regulate gene expression. Their transcriptional upregulation is associated with increased hepatic lipogenesis (Liu et al., 2012b). Instead, PPARA binds long-chain free fatty acids and is a central regulator of lipid metabolism. It heterodimerizes with RXR or LXR to regulate mitochondrial and peroxisomal fatty acid oxidation (Kersten et al., 1999; Tyagi et al., 2011; Everett et al., 2000).

Using published single-cell data from kidney (Park et al., 2018) and liver (MacParland et al., 2018), we compared the top-ranking genes defined in each study as cluster-specific markers with our pull-down enrichment results. In kidney, we found most cluster markers to be depleted following pull-down of kidney poly(A) RNA, apart from a small subset of markers for proximal tubule cells (Figure 4F). In liver, 80% of genes identified as enriched following liver poly(A) RNA pull-down were defined as markers of hepatocyte clusters.

Altogether, these results demonstrate specific labeling of renal proximal tubule epithelial cells in the kidney and of hepatocytes in the liver, with enrichment of their transcriptomes in pull-down RNA and specific depletion of genes associated with irrelevant cell types in both organs.

To assess the feasibility of detecting dynamic transcriptional responses using iTAG-RNA, we examined whether diet-induced transcriptional reprogramming can be identified in pull-down poly(A) RNA and to what extent it reflects transcriptional changes observed in whole-tissue input RNA. Differential gene expression analyses using the DESeq2 package (Love et al., 2014) revealed substantial overlap between diet-induced transcriptional reprogramming in the liver, as observed in input mRNA, and transcriptional reprogramming observed in pull-down libraries (Figure 4G; Table S3). Although the total amount of differentially expressed genes (DEGs) was roughly 4-fold lower in pull-down versus input libraries (157 versus 636 DEGs, with a false discovery rate [FDR] cutoff of less than 0.05 and an absolute $\log_2$ fold change greater than 1), a 61% overlap (96 DEGs) between the two sample sets was detected. This overlap is larger than expected by chance (chi test $< 0.0001$). Diet-induced DEGs in both input and pull-down liver RNA demonstrated significant enrichment for genes regulated by PPARA, LXR, and RXR (Figures S4A and S4C; Table S3).

As opposed to liver, diet-induced differential expression in the kidney was limited to 108 transcripts in input poly(A) RNA enriched for mitochondrial and ribosomal proteins, whereas pull-down RNA demonstrated no transcriptional reprogramming (Figures S4B and S4D; Table S3). These findings may reflect the more complex cellular composition of the kidney and a reduced sensitivity to diet-induced transcriptional reprogramming in proximal renal epithelial cells.

These results provide a proof of concept that iTAG-RNA allows isolation of cell-type-specific transcriptional responses to environmental challenges, with no need for the disruption of the tissue architecture or interference with the cellular microenvironment.

## Hepatocyte-Derived ccfRNAs Are Detected in Plasma

Given the observed hepatic transcriptional reprogramming following a HFD challenge, we examined whether we can detect labeled hepatocyte-derived RNAs in plasma and whether the profile of these secreted transcripts changes in response to the dietary challenge. Plasma-isolated ccfRNAs are predominantly short or fragmented RNA transcripts with bi-modal distribution and a major peak smaller than 200 bp (Srinivasan et al., 2019) (Figure S3G). Although we failed to generate libraries from modified plasma ccfRNAs after a single injection of HD5EU, multiple doses of HD5EU administered 6, 4, and 2 h before blood collection allowed generation of small RNA libraries following pull-down of plasma ccfRNAs.

Multiple short RNAs were pulled down in both liver and plasma under HFD and LFD (Figure 5A, 459/992 for HFD and 234/700 for LFD). This co-occurrence rate is greater than expected by chance for HFD and LFD (Figure 5A) (PV calculated using the SuperExactTest package in R; Wang et al., 2015) (fold enrichment: HFD = 2.7, LFD = 1.8; PV: HFD = 4.3e−104, LFD = 6.42e−21). The identity of pull-down plasma ccfRNAs varied between dietary challenges (Figure 5B; Tables S4 and S5), with multiple reads found enriched only under a specific dietary challenge, suggesting that liver-secreted ccfRNAs change with dietary interventions.

Various biotypes are identified in pull-down liver and plasma short RNA libraries, with the relative proportion of pull-down transcripts varying between the two. tRNAs, mitochondrial tRNAs (mt-tRNAs), and mitochondrial genes are found to be overly represented in pull-down RNA from plasma relative to liver (Figure 5C), suggesting that most mitochondrial transcripts found in plasma originate predominantly in the liver.

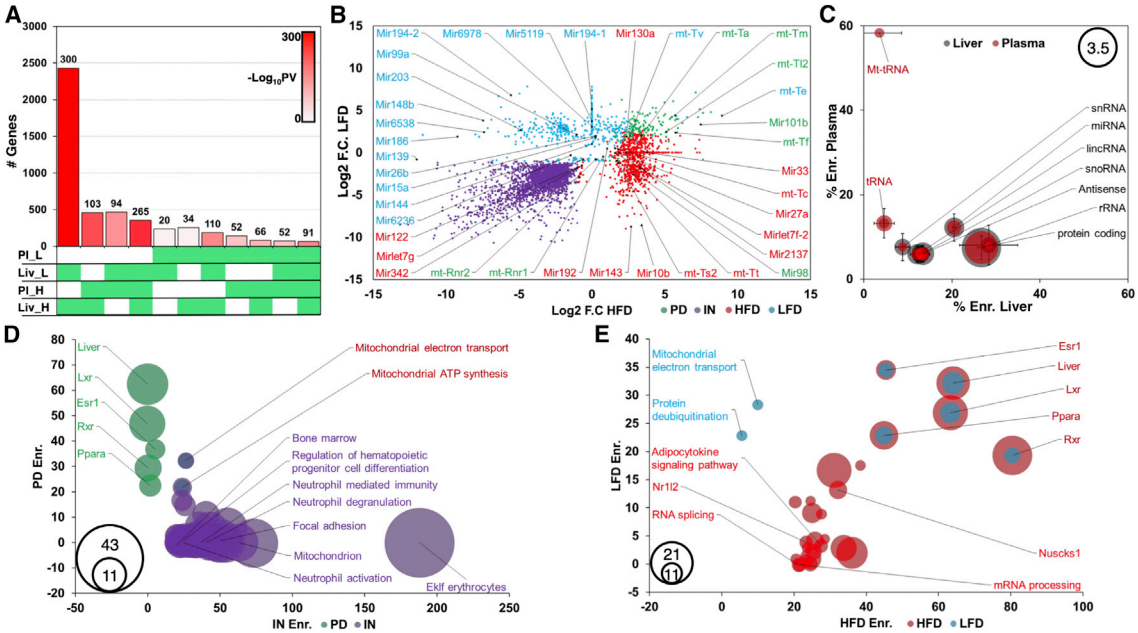


**Figure 5. Identification of Hepatocyte-Secreted Circulating Transcripts in Plasma**

(A) Overlap between pull-down small RNA transcripts in liver and plasma under HFD and LFD challenge. The number of transcripts per overlap is indicated in the y axis. Color corresponds to $-\log_{10}$ of calculated PV and is annotated in the chart. Gene sets included in each comparison are indicated in green.

(B) Scatterplot annotating selected miRNAs and mt-tRNAs identified as pulled down in circulating plasma RNA under HFD and LFD conditions. Transcripts are depleted following pull-down regardless of dietary regime (purple), pulled down regardless of dietary regime (green), or pulled down under HFD (red) or LFD (blue) only.

(C) Bubble plot representing the relative percentage of pull-down transcripts per biotype in liver and plasma libraries, averaged across HFD and LFD regimes. Bubble size represents $\log_{10}$ of the actual number of transcripts per biotype. Error bars are for SD between sets.

(D) Bubble plot of GO and gene set enrichment analysis for constitutively pull-down (green) and depleted (purple) circulating cell-free transcripts. Bubble size is proportional to $-\log_{10}$ of adj. PV.

(E) Bubble plot of GO and gene set enrichment analysis for circulating cell-free transcripts pulled down in HFD (red) or LFD (blue). Bubble size is proportional to $-\log_{10}$ of adj. PV.

Supporting the hepatic origin of plasma-labeled transcripts, circulating fragments of coding transcripts demonstrate significant enrichment for liver-specific and highly expressed genes, whereas transcripts constitutively depleted in pull-down RNA demonstrate enrichment for genes specific to bone marrow, hematopoietic differentiation, and neutrophil function (Figure 5D; Table S6). This result suggests that the hematopoietic system is one of the major contributors to the pool of circulating RNAs. HFD- and LFD-specific pull-down protein-coding transcripts demonstrate differential enrichment for annotations of adipocytokine signaling and mitochondrial electron transport, respectively (Figure 5E).

## Liver-Derived ccfRNAs Are Found in Visceral Adipose Tissue and Skeletal Muscle, Where They Buffer Cellular Response to HFD Feeding and Regulate Glucose and Lipid Homeostasis

In worms, plants, and prokaryotes, extracellular RNA signaling was described to modulate host/pathogen interactions and to orchestrate an adaptive response to environmental stimuli (Liu et al., 2012a; Weiberg et al., 2013; Timmons and Fire, 1998), and it demonstrated the idea that biological systems can exist as holobionts characterized by continuous exchange of genetic (DNA and RNA) material. In mammals, RNA-based intercellular signaling has been described in several settings (Thomou et al., 2017; Rivkin et al., 2016; Chai et al., 2017; Vickers et al., 2011; Castaño et al., 2018; Rechavi et al., 2009), using mostly *in vitro* systems or ectopic administration of RNAs to demonstrate RNA transfer and signal transduction. Little is known on the extent of RNA transfer *in vivo* and on the role it may play in physiological settings.

Two weeks of HFD feeding are sufficient to impair metabolic homeostasis (Lee et al., 2011) and induce morpho-functional alterations in both liver (Williams et al., 2014), visceral white adipose tissue (vsWAT), and skeletal muscle (Lee et al., 2011). Given the central role this triad of tissues plays in metabolic control (Hotamisligil, 2006), we used iTAG-RNA to identify a potential diet-sensitive and liver-derived RNA-based endocrine axis.

Two weeks of HFD reprogrammed transcription in both vsWAT (Figure 6A; Table S7) and skeletal muscle (gastrocnemius muscle [GAS]) (Figure 6B; Table S7), with the latter showing a more pronounced response (273 DEGs in skeletal muscle versus 131 DEGs in vsWAT inlets) (Figures 6A and 6B). Both tissues present an interesting bias toward repression of gene expression, and among the downregulated genes, an overlapping set of 11 genes (Figure 6C) include some master regulators of lipid

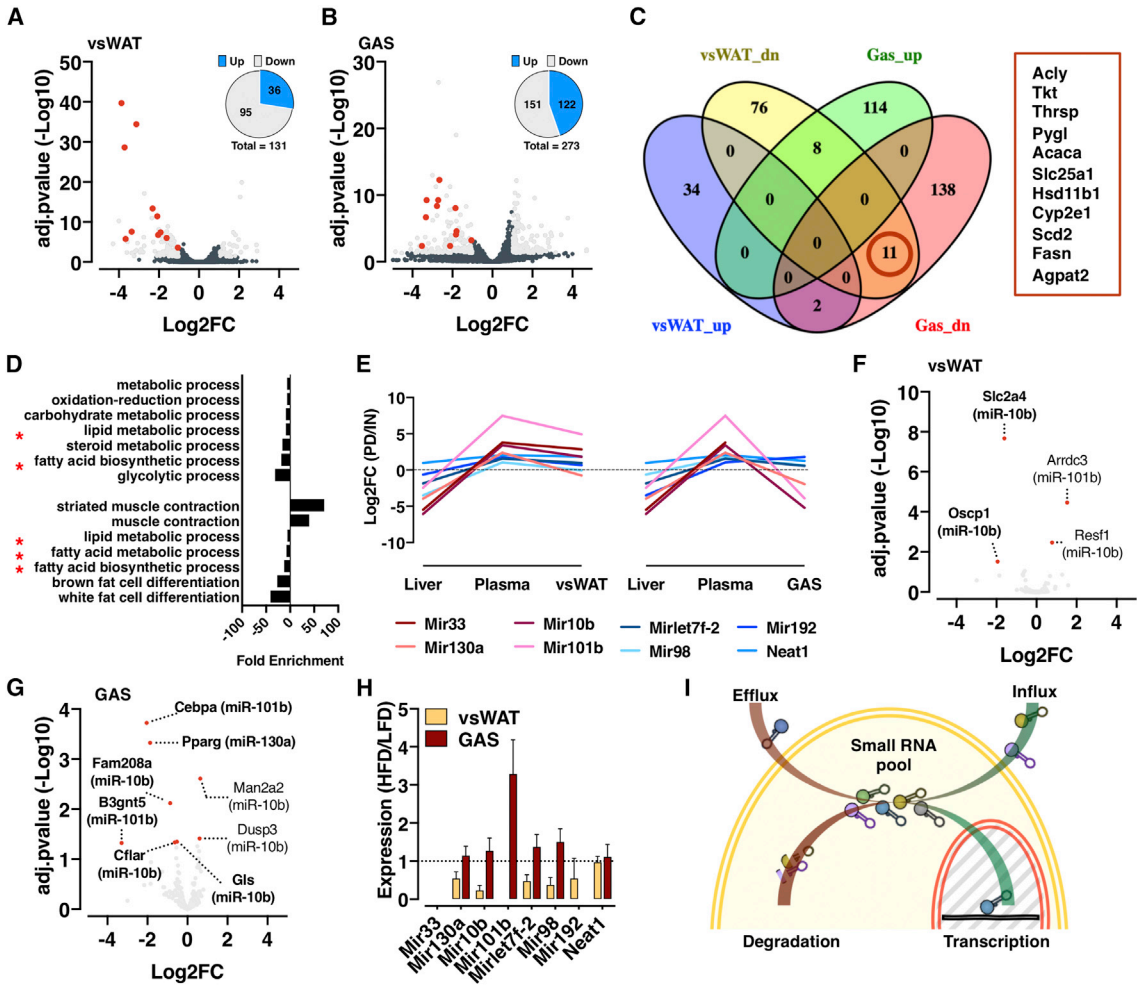


**Figure 6. Plasma ccfRNAs Can Be Detected in vsWAT and Skeletal Muscle**

(A and B) Volcano plots demonstrating DEGs in vsWAT (A) and skeletal muscle (B) upon two weeks of HFD. Red-labeled genes belong to the GO categories of lipid and fatty acid metabolic processes (also related to Table S7). Inlets show the total number of up- and downregulated genes in vsWAT and skeletal muscle.

(C) Venn diagram demonstrating overlapping DEGs between vsWAT and skeletal muscle. The 11 overlapping downregulated genes are listed in the red box and correspond to those highlighted in the volcano plots (A and B).

(D) Gene Ontology enrichment analysis of DEGs in vsWAT and skeletal muscle.

(E) Circulating miRNAs enriched in either vsWAT (left) or skeletal muscle (right).

(F and G) Volcano plots demonstrating expression and DEGs of validated target genes for the circulating miRNAs in vsWAT (F) and skeletal muscle (G).

(H) Relative expression of the identified circulating miRNAs upon two weeks of HFD in vsWAT and skeletal muscle.

(I) Model suggesting that the small RNA pool within a cell results from a balance between transcription and degradation on the one hand and influx and efflux on the other.

metabolism (such as Acly, Acaca, Scd2, Fasn, and Agpat2). Gene Ontology analysis performed on the DEGs indicates significant downregulation of lipid metabolic processes in both vsWAT and skeletal muscle (Figure 6D).

Looking for potential transfer of regulatory ccfRNAs from liver to peripheral tissues, we focused on identified hepatic transcribed ccfRNAs enriched in plasma pull-downs on HFD. We identified several liver-derived ccfRNAs in either vsWAT or skeletal muscle (Figure 6E; Table S4 ). Strikingly, transfer of miRNAs from liver to peripheral tissues is highly tissue specific. We found miR-33, miR-10b, miR-130a, and miR-101b were selectively enriched in pull-down RNAs from vsWAT, whereas miR-98 and miR-192 were specifically enriched in skeletal muscle (Figure 6E; Table S4). To understand the functional significance of liver-to-peripheral-tissue miRNA transfer, we focused on the validated targets of the identified miRNAs (as annotated by miRTarBase; Chou et al., 2018) and analyzed their expression in both vsWAT and skeletal muscle. The expression of some targets was significantly downregulated, and specific effects were observed in vsWAT and skeletal muscle (Figures 6F and 6G). For example, the insulin-dependent glucose transporter Slc2a4 (or Glut4) was specifically and strongly downregulated in vsWAT (Figure 6F; Table S4), whereas critical regulators of adipogenesis and lipid storage (such as pparg and cebpa) were specifically

downregulated in skeletal muscle (Figure 6G; Table S4). Paradoxically, every affected gene in either vsWAT or skeletal muscle is a validated target of the miRNAs specifically transferred to vsWAT (miR-10b, miR-101b, and miR-130a; see Figure 6E), which poses a question about the physiological significance of the identified RNA transfer.

To solve this paradox, we analyzed the endogenous expression of the identified miRNAs in vsWAT and skeletal muscle and found that their expression is differently and tissue-specifically regulated by the HFD. In particular, although either not affected (miR-130a and miR-10b) or upregulated (miR-101b) in skeletal muscle (Figure 6H), miRNAs specifically transferred to vsWAT were significantly suppressed by HFD in vsWAT (Figure 6H).

Altogether, these findings identify a diet-sensitive RNA-based endocrine axis on which hepatocyte-transcribed regulatory RNAs are selectively transferred to peripheral tissues to buffer endogenous transcriptional responses and maintain homeostasis.

## DISCUSSION

Studying the role of circulating RNAs in endocrine signaling has been limited by the lack of a method that would allow specific and unbiased labeling of cellular transcription and tracking of circulating RNAs from the transcriptional source to their functional sink. Here, we present iTAG-RNA, a method for targeted *in vivo* labeling of global RNA transcription, and use it to identify hepatocyte-secreted ccfRNAs and their uptake by peripheral tissues *in vivo*. iTAG-RNA allows labeling of total RNA transcripts *in vivo* using two main components: HD5EU, a newly designed small molecule that serves as a substrate for the human CYP3A4 enzyme, and an existing humanized transgenic mouse model expressing the human CYP3A4 enzyme under a modified APOE promoter (Figure 1). CYP3A4 catalyzes the oxidative cleavage of an aryl group of the HD5EU molecule, which in turn undergoes spontaneous beta elimination to produce a bioavailable 5EU monophosphate. The existing transgenic mouse model allows *in vivo* labeling of hepatocytes and kidney proximal renal epithelial cells (Figure 2), because the tissue expression pattern of the enzyme dictates the site of the small molecule's metabolism and subsequent RNA labeling. To validate the specificity of HD5EU metabolism, we demonstrate that the molecule is indeed metabolized in a CYP3A4-dependent manner to 5EU monophosphate, which is then incorporated in place of uridine into transcribing RNA (Figures 2 and 3) and allows highly selective RNA precipitation and sequencing of labeled RNAs (Figure 4A; Figure S3). Further development of transgenic models would allow labeling of any tissue and analysis of tissue-specific circulating RNAs.

Administration of HD5EU allows enrichment for the transcriptional program of proximal renal epithelial cells and hepatocytes *in situ* without disruption of the kidney or liver architecture (Figures 4B–4G), which is critical to maintaining tissue homeostasis and preventing transcriptional alterations secondary to tissue manipulations. In addition, environmentally induced transcriptional reprogramming is evident following labeling (Figure S4). As opposed to recently described methods (Alberti et al., 2018; Gay et al., 2013; Hida et al., 2017; Miller et al., 2009), and in keeping with the literature in which RNA Pol I, RNA Pol II, and RNA Pol III are demonstrated to incorporate 5EU (Jao and Salic, 2008), mRNA and small RNAs of various types, including rRNA, tRNA, and miRNA, are found to be labeled and enriched in pull-down RNA.

Critically, and uniquely to iTAG-RNA, we are also able to enrich for liver-derived plasma ccfRNAs following administration of multiple doses of HD5EU (Figure 5). Pull-down plasma ccfRNAs demonstrate enrichment for liver-derived RNA fragments of protein-coding genes, whereas depleted transcripts demonstrate enrichment for annotations relating to function and differentiation of the hematopoietic system. Apart from fragments of protein-coding genes, liver-secreted ccfRNA include various small RNA transcripts, such as miRNAs, mt-tRNAs, and tRNAs. Given the evident enrichment for mitochondrial transcripts following pull-down, our results suggest that hepatocytes are the main source of mitochondrially encoded ccfRNA transcripts in plasma. Although the function of these transcripts remains to be elucidated, several studies have suggested that tRNAs and tRNA fragments can mediate cellular signaling and that the overall tRNA pool and composition within a cell has functional significance (Kirchner and Ignatova, 2015). To date, most potential ccfRNA biomarkers associated with liver pathologies have been miRNAs (Enache et al., 2014). Our findings suggest that fragments of protein-coding genes, together with mt-tRNAs and mitochondrially encoded transcripts, can also potentially be useful biomarkers for hepatic function.

RNA molecules can circulate in plasma and other biological fluids either freely or in lipoprotein complexes (Murillo et al., 2019; Yeri et al., 2017), the best known of which are exosomes, extracellular vesicles, and high- and low-density lipoproteins. Although not tested, we expect homogeneous distribution across the aforementioned particles of liver-secreted RNAs, in keeping with their hepatocyte origin (Deng et al., 2017) and their diversity and non-specificity of RNA loading (Donker et al., 2012; Tosar et al., 2015).

To fully understand the role of circulating RNAs in intercellular communication, it is critical to track them from their transcriptional source to the functional sink. Therefore, we analyzed transfer of liver-derived RNAs to vsWAT and skeletal muscle (GAS), and we did it in response to an acute HFD challenge to identify a potential physiologically relevant RNA-based endocrine axis. Despite not being technically able to dissect RNA transfer at single-cell resolution and identify the recipient cell type in the target tissues, we detected transfer of liver-derived transcripts to both vsWAT and GAS in response to diet (Figure 6E). Although both tissues responded similarly to the dietary challenge by downregulating genes involved in lipid metabolism and fatty acid biosynthesis (Figures 6A–6D), we identified specific transfer of liver-derived miRNAs to either vsWAT (miR33, miR-10b, miR-130a, and miR-101b) or skeletal muscle (miR-98 and miR-192) (Figure 6E), and significant downregulation of miR-10b, miR-130a, and miR-101b validated target genes in both tissues (Figures 6F and 6G). Thus, although not transferred to skeletal muscle, these miRNAs seem to be important to regulate transcriptional response to HFD in both tissues. Importantly, we have also shown that the endogenous expression of these

miRNAs responds to the HFD in a tissue-specific manner (Figure 6H). Altogether, our findings suggest that the intracellular pool of small RNAs *in vivo* results from a tight balance not only between transcription and degradation but also between influx and efflux of small RNAs from the extracellular milieu (Figure 6I), all serving as a buffering mechanism for transcriptional and physiological responses in target cells.

Thus, iTAG-RNA isolates cellular transcriptional responses to dietary challenge *in vivo* and, without tissue dissociation, identifies hepatocyte-secreted transcripts, finally tracking them from source to sink. Lastly, our findings suggest a function for circulating transcripts in buffering cellular transcriptional responses to an environmental challenge to maintain homeostasis.

Although our analysis has been limited to the most immediately relevant tissues for the applied environmental challenge, iTAG-RNA offers the opportunity to study liver-based intercellular communication to distant tissue. In addition, further developments of the method with implementation of new tissue-specific knockins for hCYP3A4 would allow the construction of an RNA-based endocrine network and the study of its function in health and disease in mammals.

## STAR★METHODS

Detailed methods are provided in the online version of this paper and include the following:

- KEY RESOURCES TABLE
- LEAD CONTACT AND MATERIALS AVAILABILITY
- EXPERIMENTAL MODEL AND SUBJECT DETAILS
  - Mice handling
  - Cell culture
- METHOD DETAILS
  - Tissue processing and imaging
  - Western Blot
  - RNA extraction and qRT-PCR
  - RNA pull-down and library construction
  - UPLC-UHR-ToF-MS analysis
- QUANTIFICATION AND STATISTICAL ANALYSIS
  - Bioinformatic analysis
- DATA AND CODE AVAILABILITY

## SUPPLEMENTAL INFORMATION

Supplemental Information can be found online at https://doi.org/10.1016/j.celrep.2020.02.020.

## ACKNOWLEDGMENTS

We thank Dr. Julia Calzada-Wack, Jacqueline Mueller, and Marion Fisch for their assistance with tissue processing and sectioning. We thank Dr. Anja Zeigerer for access to and assistance with the confocal microscope. This work has been supported by the German Diabetes Research Center (DZD NEXT Grant 2019) to R.T. and by the ERC Recognition Award from the Helmholtz Research Center Munich to R.T. The authors thank the Helmholtz Association and the German Diabetes Research Center for funding the positions of R.G., J.D., M.L., F.S., A.T., L.B., A.H., and R.T.

## AUTHOR CONTRIBUTIONS

Conceptualization, Y.D.; Methodology, Y.D. and M.W.; Investigation, Y.D., M.L., R.G., A.T., F.S., L.B., A.H., and M.W.; Data Analysis, J.D., A.T., M.W., and R.T.; Writing – Original Draft, Y.D., M.W., and R.T.; Writing – Review & Editing, Y.D., M.H.d.A., M.W., and R.T.; Funding Acquisition, M.H.d.A. and R.T.; Resources, M.H.d.A., M.W., and R.T.; Supervision, R.T.

## DECLARATION OF INTERESTS

The authors declare no competing interests.

Received: June 18, 2019
Revised: December 6, 2019
Accepted: February 5, 2020
Published: March 3, 2020

## REFERENCES

Alberti, C., Manzenreither, R.A., Sowemimo, I., Burkard, T.R., Wang, J., Mahofsky, K., Ameres, S.L., and Cochella, L. (2018). Cell-type specific sequencing of microRNAs from complex animal tissues. Nat. Methods *15*, 283–289.

Best, M.D. (2009). Click chemistry and bioorthogonal reactions: unprecedented selectivity in the labeling of biological molecules. Biochemistry *48*, 6571–6584.

Boyer, S.H., Sun, Z., Jiang, H., Esterbrook, J., Gómez-Galeno, J.E., Craigo, W., Reddy, K.R., Ugarkar, B.G., MacKenna, D.A., and Erion, M.D. (2006). Synthesis and characterization of a novel liver-targeted prodrug of cytosine-1-beta-D-arabinofuranoside monophosphate for the treatment of hepatocellular carcinoma. J. Med. Chem. *49*, 7711–7720.

Castaño, C., Kalko, S., Novials, A., and Párrizas, M. (2018). Obesity-associated exosomal miRNAs modulate glucose and lipid metabolism in mice. Proc. Natl. Acad. Sci. USA *115*, 12158–12163.

Chai, C., Rivkin, M., Berkovits, L., Simerzin, A., Zorde-Khvalevsky, E., Rosenberg, N., Klein, S., Yaish, D., Durst, R., Shpitzen, S., et al. (2017). Metabolic Circuit Involving Free Fatty Acids, microRNA 122, and Triglyceride Synthesis in Liver and Muscle Tissues. Gastroenterology *153*, 1404–1415.

Chan, P.P., and Lowe, T.M. (2016). GtRNAdb 2.0: an expanded database of transfer RNA genes identified in complete and draft genomes. Nucleic Acids Res. *44* (*D1*), D184–D189.

Chatzi, C., Zhang, Y., Shen, R., Westbrook, G.L., and Goodman, R.H. (2016). Transcriptional Profiling of Newly Generated Dentate Granule Cells Using TU Tagging Reveals Pattern Shifts in Gene Expression during Circuit Integration. eNeuro *3*, ENEURO.0024-16.2016.

Chen, E.Y., Tan, C.M., Kou, Y., Duan, Q., Wang, Z., Meirelles, G.V., Clark, N.R., and Ma'ayan, A. (2013). Enrichr: interactive and collaborative HTML5 gene list enrichment analysis tool. BMC Bioinformatics *14*, 128.

Chou, C.H., Shrestha, S., Yang, C.D., Chang, N.W., Lin, Y.L., Liao, K.W., Huang, W.C., Sun, T.H., Tu, S.J., Lee, W.H., et al. (2018). miRTarBase update 2018: a resource for experimentally validated microRNA-target interactions. Nucleic Acids Res. *46* (*D1*), D296–D302.

Coudrier, E., Kerjaschki, D., and Louvard, D. (1988). Cytoskeleton organization and submembranous interactions in intestinal and renal brush borders. Kidney Int. *34*, 309–320.

Deng, F., Magee, N., and Zhang, Y. (2017). Decoding the Role of Extracellular Vesicles in Liver Diseases. Liver Res. *1*, 147–155.

Dobin, A., Davis, C.A., Schlesinger, F., Drenkow, J., Zaleski, C., Jha, S., Batut, P., Chaisson, M., and Gingeras, T.R. (2013). STAR: ultrafast universal RNA-seq aligner. Bioinformatics *29*, 15–21.

Donker, R.B., Mouillet, J.F., Chu, T., Hubel, C.A., Stolz, D.B., Morelli, A.E., and Sadovsky, Y. (2012). The expression profile of C19MC microRNAs in primary human trophoblast cells and exosomes. Mol. Hum. Reprod. *18*, 417–424.

Dror, S., Sander, L., Schwartz, H., Sheinboim, D., Barzilai, A., Dishon, Y., Apcher, S., Golan, T., Greenberger, S., Barshack, I., et al. (2016). Melanoma miRNA trafficking controls tumour primary niche formation. Nat. Cell Biol. *18*, 1006–1017.

Enache, L.S., Enache, E.L., Ramière, C., Diaz, O., Bancu, L., Sin, A., and André, P. (2014). Circulating RNA molecules as biomarkers in liver disease. Int. J. Mol. Sci. *15*, 17644–17666.

Erion, M.D., Reddy, K.R., Boyer, S.H., Matelich, M.C., Gomez-Galeno, J., Lemus, R.H., Ugarkar, B.G., Colby, T.J., Schanzer, J., and Van Poelje, P.D. (2004). Design, synthesis, and characterization of a series of cytochrome P(450) 3A-activated prodrugs (HepDirect prodrugs) useful for targeting phosph(on)ate-based drugs to the liver. J. Am. Chem. Soc. *126*, 5154–5163.

Erion, M.D., Cable, E.E., Ito, B.R., Jiang, H., Fujitaki, J.M., Finn, P.D., Zhang, B.H., Hou, J., Boyer, S.H., van Poelje, P.D., and Linemeyer, D.L. (2007). Targeting thyroid hormone receptor-beta agonists to the liver reduces cholesterol and triglycerides and improves the therapeutic index. Proc. Natl. Acad. Sci. USA *104*, 15490–15495.

Everett, L., Galli, A., and Crabb, D. (2000). The role of hepatic peroxisome proliferator-activated receptors (PPARs) in health and disease. Liver *20*, 191–199.

Fina, L., Molgaard, H.V., Robertson, D., Bradley, N.J., Monaghan, P., Delia, D., Sutherland, D.R., Baker, M.A., and Greaves, M.F. (1990). Expression of the CD34 gene in vascular endothelial cells. Blood *75*, 2417–2426.

Gay, L., Miller, M.R., Ventura, P.B., Devasthali, V., Vue, Z., Thompson, H.L., Temple, S., Zong, H., Cleary, M.D., Stankunas, K., and Doe, C.Q. (2013). Mouse TU tagging: a chemical/genetic intersectional method for purifying cell type-specific nascent RNA. Genes Dev. *27*, 98–115.

Ghosh, A.C., Shimell, M., Leof, E.R., Haley, M.J., and O'Connor, M.B. (2015). UPRT, a suicide-gene therapy candidate in higher eukaryotes, is required for *Drosophila* larval growth and normal adult lifespan. Sci. Rep. *5*, 13176.

Gierlich, J., Burley, G.A., Gramlich, P.M., Hammond, D.M., and Carell, T. (2006). Click chemistry as a reliable method for the high-density postsynthetic functionalization of alkyne-modified DNA. Org. Lett. *8*, 3639–3642.

Gilad, S., Meiri, E., Yogev, Y., Benjamin, S., Lebanony, D., Yerushalmi, N., Benjamin, H., Kushnir, M., Cholakh, H., Melamed, N., et al. (2008). Serum microRNAs are promising novel biomarkers. PLoS ONE *3*, e3148.

Hagemeijer, M.C., Vonk, A.M., Monastyrska, I., Rottier, P.J., and de Haan, C.A. (2012). Visualizing coronavirus RNA synthesis in time by using click chemistry. J. Virol. *86*, 5808–5816.

Herzog, V.A., Reichholf, B., Neumann, T., Rescheneder, P., Bhat, P., Burkard, T.R., Wlotzka, W., von Haeseler, A., Zuber, J., and Ameres, S.L. (2017). Thiol-linked alkylation of RNA to assess expression dynamics. Nat. Methods *14*, 1198–1204.

Hida, N., Aboukilila, M.Y., Burow, D.A., Paul, R., Greenberg, M.M., Fazio, M., Beasley, S., Spitale, R.C., and Cleary, M.D. (2017). EC-tagging allows cell type-specific RNA analysis. Nucleic Acids Res. *45*, e138.

Hotamisligil, G.S. (2006). Inflammation and metabolic disorders. Nature *444*, 860–867.

Jao, C.Y., and Salic, A. (2008). Exploring RNA transcription and turnover *in vivo* by using click chemistry. Proc. Natl. Acad. Sci. USA *105*, 15779–15784.

Kersten, S., Seydoux, J., Peters, J.M., Gonzalez, F.J., Desvergne, B., and Wahli, W. (1999). Peroxisome proliferator-activated receptor alpha mediates the adaptive response to fasting. J. Clin. Invest. *103*, 1489–1498.

Kirchner, S., and Ignatova, Z. (2015). Emerging roles of tRNA in adaptive translation, signalling dynamics and disease. Nat. Rev. Genet. *16*, 98–112.

Kosaka, N., Iguchi, H., Yoshioka, Y., Takeshita, F., Matsuki, Y., and Ochiya, T. (2010). Secretory mechanisms and intercellular transfer of microRNAs in living cells. J. Biol. Chem. *285*, 17442–17452.

Lee, Y.S., Li, P., Huh, J.Y., Hwang, I.J., Lu, M., Kim, J.I., Ham, M., Talukdar, S., Chen, A., Lu, W.J., et al. (2011). Inflammation is necessary for long-term but not short-term high-fat diet-induced insulin resistance. Diabetes *60*, 2474–2483.

Lin, G., Finger, E., and Gutierrez-Ramos, J.C. (1995). Expression of CD34 in endothelial cells, hematopoietic progenitors and nervous cells in fetal and adult mouse tissues. Eur. J. Immunol. *25*, 1508–1516.

Liu, H., Wang, X., Wang, H.D., Wu, J., Ren, J., Meng, L., Wu, Q., Dong, H., Wu, J., Kao, T.Y., et al. (2012a). *Escherichia coli* noncoding RNAs can affect gene expression and physiology of *Caenorhabditis elegans*. Nat. Commun. *3*, 1073.

Liu, Y., Qiu, D.K., and Ma, X. (2012b). Liver X receptors bridge hepatic lipid metabolism and inflammation. J. Dig. Dis. *13*, 69–74.

Love, M.I., Huber, W., and Anders, S. (2014). Moderated estimation of fold change and dispersion for RNA-seq data with DESeq2. Genome Biol. *15*, 550.

MacParland, S.A., Liu, J.C., Ma, X.Z., Innes, B.T., Bartczak, A.M., Gage, B.K., Manuel, J., Khuu, N., Echeverri, J., Linares, I., et al. (2018). Single cell RNA sequencing of human liver reveals distinct intrahepatic macrophage populations. Nat. Commun. *9*, 4383.

Maquat, L.E., and Kiledjian, M. (2008). RNA turnover in eukaryotes: nucleases, pathways and analysis of mRNA decay. Preface. Methods Enzymol. *448*, xxi–xxii.

Marquart, T.J., Allen, R.M., Ory, D.S., and Baldán, A. (2010). miR-33 links SREBP-2 induction to repression of sterol transporters. Proc. Natl. Acad. Sci. USA *107*, 12228–12232.

Martin, M. (2011). Cutadapt removes adapter sequences from high-throughput sequencing reads. EMBnet J. *17*, 10–12.

Meyer, J.P., Adumeau, P., Lewis, J.S., and Zeglis, B.M. (2016). Click Chemistry and Radiochemistry: The First 10 Years. Bioconjug. Chem. *27*, 2791–2807.

Miller, M.R., Robinson, K.J., Cleary, M.D., and Doe, C.Q. (2009). TU-tagging: cell type-specific RNA isolation from intact complex tissues. Nat. Methods *6*, 439–441.

Murillo, O.D., Thistlethwaite, W., Rozowsky, J., Subramanian, S.L., Lucero, R., Shah, N., Jackson, A.R., Srinivasan, S., Chung, A., Laurent, C.D., et al. (2019). exRNA Atlas Analysis Reveals Distinct Extracellular RNA Cargo Types and Their Carriers Present across Human Biofluids. Cell *177*, 463–477.

Park, J., Shrestha, R., Qiu, C., Kondo, A., Huang, S., Werth, M., Li, M., Barasch, J., and Suszták, K. (2018). Single-cell transcriptomics of the mouse kidney reveals potential cellular targets of kidney disease. Science *360*, 758–763.

Pastuzyn, E.D., Day, C.E., Kearns, R.B., Kyrke-Smith, M., Taibi, A.V., McCormick, J., Yoder, N., Belnap, D.M., Erlendsson, S., Morado, D.R., et al. (2018). The Neuronal Gene Arc Encodes a Repurposed Retrotransposon Gag Protein that Mediates Intercellular RNA Transfer. Cell *172*, 275–288.

Pegtel, D.M., Cosmopoulos, K., Thorley-Lawson, D.A., van Eijndhoven, M.A., Hopmans, E.S., Lindenberg, J.L., de Gruijl, T.D., Würdinger, T., and Middeldorp, J.M. (2010). Functional delivery of viral miRNAs via exosomes. Proc. Natl. Acad. Sci. USA *107*, 6328–6333.

Pradere, U., Garnier-Amblard, E.C., Coats, S.J., Amblard, F., and Schinazi, R.F. (2014). Synthesis of nucleoside phosphate and phosphonate prodrugs. Chem. Rev. *114*, 9154–9218.

Rayner, K.J., Suárez, Y., Dávalos, A., Parathath, S., Fitzgerald, M.L., Tamehiro, N., Fisher, E.A., Moore, K.J., and Fernández-Hernando, C. (2010). MiR-33 contributes to the regulation of cholesterol homeostasis. Science *328*, 1570–1573.

Rechavi, O., Erlich, Y., Amram, H., Flomenblit, L., Karginov, F.V., Goldstein, I., Hannon, G.J., and Kloog, Y. (2009). Cell contact-dependent acquisition of cellular and viral nonautonomously encoded small RNAs. Genes Dev. *23*, 1971–1979.

Reddy, K.R., Matelich, M.C., Ugarkar, B.G., Gómez-Galeno, J.E., DaRe, J., Ollis, K., Sun, Z., Craigo, W., Colby, T.J., Fujitaki, J.M., et al. (2008). Pradefovir: a prodrug that targets adefovir to the liver for the treatment of hepatitis B. J. Med. Chem. *51*, 666–676.

Rivkin, M., Simerzin, A., Zorde-Khvalevsky, E., Chai, C., Yuval, J.B., Rosenberg, N., Harari-Steinfeld, R., Schneider, R., Amir, G., Condiotti, R., et al. (2016). Inflammation-Induced Expression and Secretion of MicroRNA 122 Leads to Reduced Blood Levels of Kidney-Derived Erythropoietin and Anemia. Gastroenterology *151*, 999–1010.

Schwarzenbach, H., Nishida, N., Calin, G.A., and Pantel, K. (2014). Clinical relevance of circulating cell-free microRNAs in cancer. Nat. Rev. Clin. Oncol. *11*, 145–156.

Sharma, U., Sun, F., Conine, C.C., Reichholf, B., Kukreja, S., Herzog, V.A., Ameres, S.L., and Rando, O.J. (2018). Small RNAs Are Trafficked from the Epididymis to Developing Mammalian Sperm. Dev. Cell *46*, 481–494.

Simonet, W.S., Bucay, N., Lauer, S.J., and Taylor, J.M. (1993). A far-downstream hepatocyte-specific control region directs expression of the linked human apolipoprotein E and C-I genes in transgenic mice. J. Biol. Chem. *268*, 8221–8229.

Song, A.J., and Palmiter, R.D. (2018). Detecting and Avoiding Problems When Using the Cre-lox System. Trends Genet. *34*, 333–340.

Srinivasan, S., Yeri, A., Cheah, P.S., Chung, A., Danielson, K., De Hoff, P., Filant, J., Laurent, C.D., Laurent, L.D., Magee, R., et al. (2019). Small RNA Sequencing across Diverse Biofluids Identifies Optimal Methods for exRNA Isolation. Cell *177*, 446–462.

Stresser, D.M., Broudy, M.I., Ho, T., Cargill, C.E., Blanchard, A.P., Sharma, R., Dandeneau, A.A., Goodwin, J.J., Turner, S.D., Erve, J.C., et al. (2004). Highly selective inhibition of human CYP3Aa *in vitro* by azamulin and evidence that inhibition is irreversible. Drug Metab. Dispos. *32*, 105–112.

Su, D., Chan, C.T., Gu, C., Lim, K.S., Chionh, Y.H., McBee, M.E., Russell, B.S., Babu, I.R., Begley, T.J., and Dedon, P.C. (2014). Quantitative analysis of ribonucleoside modifications in tRNA by HPLC-coupled mass spectrometry. Nat. Protoc. *9*, 828–841.

Tarazona, S., García-Alcalde, F., Dopazo, J., Ferrer, A., and Conesa, A. (2011). Differential expression in RNA-seq: a matter of depth. Genome Res. *21*, 2213–2223.

Tarazona, S., Furió-Tarí, P., Turrà, D., Pietro, A.D., Nueda, M.J., Ferrer, A., and Conesa, A. (2015). Data quality aware analysis of differential expression in RNA-seq with NOISeq R/Bioc package. Nucleic Acids Res. *43*, e140.

Thomou, T., Mori, M.A., Dreyfuss, J.M., Konishi, M., Sakaguchi, M., Wolfrum, C., Rao, T.N., Winnay, J.N., Garcia-Martin, R., Grinspoon, S.K., et al. (2017). Adipose-derived circulating miRNAs regulate gene expression in other tissues. Nature *542*, 450–455.

Timmons, L., and Fire, A. (1998). Specific interference by ingested dsRNA. Nature *395*, 854.

Tosar, J.P., Gámbaro, F., Sanguinetti, J., Bonilla, B., Witwer, K.W., and Cayota, A. (2015). Assessment of small RNA sorting into different extracellular fractions revealed by high-throughput sequencing of breast cell lines. Nucleic Acids Res. *43*, 5601–5616.

Tyagi, S., Gupta, P., Saini, A.S., Kaushal, C., and Sharma, S. (2011). The peroxisome proliferator-activated receptor: A family of nuclear receptors role in various diseases. J. Adv. Pharm. Technol. Res. *2*, 236–240.

van Herwaarden, A.E., Smit, J.W., Sparidans, R.W., Wagenaar, E., van der Kruijssen, C.M., Schellens, J.H., Beijnen, J.H., and Schinkel, A.H. (2005). Midazolam and cyclosporin a metabolism in transgenic mice with liver-specific expression of human CYP3A4. Drug Metab. Dispos. *33*, 892–895.

van Herwaarden, A.E., Wagenaar, E., van der Kruijssen, C.M., van Waterschoot, R.A., Smit, J.W., Song, J.Y., van der Valk, M.A., van Tellingen, O., van der Hoorn, J.W., Rosing, H., et al. (2007). Knockout of cytochrome P450 3A yields new mouse models for understanding xenobiotic metabolism. J. Clin. Invest. *117*, 3583–3592.

Vickers, K.C., Palmisano, B.T., Shoucri, B.M., Shamburek, R.D., and Remaley, A.T. (2011). MicroRNAs are transported in plasma and delivered to recipient cells by high-density lipoproteins. Nat. Cell Biol. *13*, 423–433.

Wang, M., Zhao, Y., and Zhang, B. (2015). Efficient Test and Visualization of Multi-Set Intersections. Sci. Rep. *5*, 16923.

Weiberg, A., Wang, M., Lin, F.M., Zhao, H., Zhang, Z., Kaloshian, I., Huang, H.D., and Jin, H. (2013). Fungal small RNAs suppress plant immunity by hijacking host RNA interference pathways. Science *342*, 118–123.

Williams, L.M., Campbell, F.M., Drew, J.E., Koch, C., Hoggard, N., Rees, W.D., Kamolrat, T., Thi Ngo, H., Steffensen, I.L., Gray, S.R., and Tups, A. (2014). The development of diet-induced obesity and glucose intolerance in C57BL/6 mice on a high-fat diet consists of distinct phases. PLoS ONE *9*, e106159.

Wortzel, I., Dror, S., Kenific, C.M., and Lyden, D. (2019). Exosome-Mediated Metastasis: Communication from a Distance. Dev. Cell *49*, 347–360.

Yeri, A., Courtright, A., Reiman, R., Carlson, E., Beecroft, T., Janss, A., Siniard, A., Richholt, R., Balak, C., Rozowsky, J., et al. (2017). Total Extracellular Small RNA Profiles from Plasma, Saliva, and Urine of Healthy Subjects. Sci. Rep. *7*, 44061.

Zerbino, D.R., Achuthan, P., Akanni, W., Amode, M.R., Barrell, D., Bhai, J., Billis, K., Cummins, C., Gall, A., Girón, C.G., et al. (2018). Ensembl 2018. Nucleic Acids Res. *46* (*D1*), D754–D761.

## STAR★METHODS

### KEY RESOURCES TABLE

| REAGENT or RESOURCE | SOURCE | IDENTIFIER |
|---|---|---|
| Antibodies | | |
| anti-CYP3A4 | Thermo Fisher | Cat#MA5-17064; RRID: AB_2538535 |
| Phospho-p53 (Ser392) Antibody | cell signaling | Cat#9281; RRID: AB_331462 |
| anti-total-p53 | cell signaling | Cat#2524; RRID: AB_331743 |
| Anti-Cleaved Caspase-3 antibody | abcam | Cat#ab214430 |
| Anti-Caspase-3 antibody | abcam | Cat#ab184787 |
| anti-HSP90 | Santa-Cruz | Cat#SC-7949 |
| Anti-mouse IgG, HRP-linked Antibody | Cell signaling | Cat#7076 |
| Anti-rabbit IgG, HRP-linked Antibody | Cell signaling | Cat#7074 |
| Chemicals, Peptides, and Recombinant Proteins | | |
| adenosine | Sigma-Aldrich | Cat#A9251 |
| guanosine | Sigma-Aldrich | Cat#G6752 |
| cytidine | Sigma-Aldrich | Cat#C4654 |
| uridine | Sigma-Aldrich | Cat#U3750 |
| 5-Ethynyl uridine (5EU) | Carl Roth | Cat#7848.2 |
| HepDirect 5EU (HD5EU) | ChiroBlock GmbH | Custom synthesis – no catalog number available |
| Phosphatase, Alkaline from bovine intestinal mucosa | Sigma-Aldrich | Cat#P5521 |
| Phosphodiesterase I from *Crotalus adamanteus* venom | Sigma-Aldrich | Cat#P3243 |
| Benzonase | Sigma-Aldrich | Cat#E8263 |
| PEG-400 | Sigma-Aldrich | Cat# 91893-250ML-F |
| NaCl 0.9% | Sigma-Aldrich | Cat# S8776 |
| DMSO | Sigma-Aldrich | Cat#41639 |
| Liver perfusion buffer | GIBCO | Cat#17701-038 |
| Liver digestion buffer | GIBCO | Cat#17703-034 |
| Geltrex | Thermo Fisher | Cat#A1413201 |
| Williams' Medium E | GIBCO | Cat#A12176 |
| Primary Hepatocyte Maintenance Supplements | GIBCO | Cat#CM4000 |
| Azamulin | Sigma-Aldrich | Cat#SML0485 |
| UltraPure Glycogen | Thermo Fisher | Cat#10814010 |
| Bolt 4-12% Bis-Tris Plus gradient Gels | Invitrogen | Cat#NW04120 |
| 20X Bolt MOPS SDS Running Buffer | Invitrogen | Cat#B0001 |
| Bolt Transfer Buffer (20X) | Invitrogen | Cat#BT0006 |
| iBind Solution Kit | Invitrogen | Cat#SLF1020 |
| Critical Commercial Assays | | |
| Click-iT RNA Alexa Fluor 594 Imaging Kit | Thermo Fisher | Cat#C10330 |
| Pierce ECL Western Blotting Substrate | Thermo Fisher | Cat#32209 |
| TRI Reagent BD | Sigma-Aldrich | Cat#T3809 |
| NucleoZOL | Macherey-Nagel | Cat#740404.200 |
| Click-it Nascent RNA Capture Kit | Thermo Fisher | Cat#C10365 |
| CATS mRNA-seq Kit, with polyA selection | Diagenode | Cat#C05010043 |
| CATS small RNA kit | Diagenode | Cat#C05010040 |
| High-Capacity cDNA Reverse Transcription Kit | Thermo Fisher | Cat#4368814 |
| SYBR Green PCR Master Mix | applied biosystems | Cat#4309155 |

(*Continued on next page*)

| Continued | | |
|---|---|---|
| REAGENT or RESOURCE | SOURCE | IDENTIFIER |
| Deposited Data | | |
| Deposited sequencing data | Gene Expression Omnibus | GSE143562 |
| Single cell RNA sequencing of human liver. | MacParland et al., 2018 | GSE115469 |
| Single-cell transcriptomics of the mouse kidney. | Park et al., 2018 | GSE107585 |
| Experimental Models: Organisms/Strains | | |
| model organism: hCYP3A4 mice; genotype: "Mouse: *Cyp3a13*$^{tm1Ahs}$ Del(5Cyp3a57-Cyp3a59)1Ahs Tg(APOE-CYP3A4)A1Ah" | Taconic | Cat#9048 |
| Oligonucleotides | | |
| hCyp3-F - TTGGCATGAGGTTTGCTCTC | This paper | N/A |
| hCyp3-R - ACAACGGGTTTTTCTGGTTG | This paper | N/A |
| Actin-F - CACAGCTTCTTTGCAGCTCCT | This paper | N/A |
| Actin-R - CAGCAGTGCAATGTTAAAAGG | This paper | N/A |
| Software and Algorithms | | |
| GraphPad Prism 8.3.1 | GraphPad | https://www.graphpad.com/ |
| STAR aligner | Dobin et al., 2013 | https://github.com/alexdobin/STAR |
| Galaxy | | https://usegalaxy.org |
| HTSeq | | https://pypi.org/project/HTSeq/ |
| DESeq2 | Love et al., 2014 | http://bioconductor.org/packages/release/bioc/html/DESeq2.html |
| NOISeq | Tarazona et al., 2011 | http://www.bioconductor.org/packages/release/bioc/html/NOISeq.html |
| SuperExactTest R Package | Wang et al., 2015 | https://cran.r-project.org/web/packages/SuperExactTest/index.html |
| Cutadapt | Martin, 2011 | https://cutadapt.readthedocs.io/en/stable/ |
| EnrichR | Chen et al., 2013 | https://amp.pharm.mssm.edu/Enrichr/ |
| Other | | |
| Rodent Diet with 60 kcal% from fat | Research Diets | Cat#D12492i |
| Rodent Diet with 10 kcal% from fat | Research Diets | Cat#D12450B |

## LEAD CONTACT AND MATERIALS AVAILABILITY

Any information request on this study should be addressed to the Lead Contact, Raffaele Teperino, PhD (raffaele.teperino@helmholtz-muenchen.de). This study did not generate new unique reagents. HD5EU is available for purchase from ChiroBlock GmbH. hCyp3A4 animals are available for purchase from TACONIC Inc.

## EXPERIMENTAL MODEL AND SUBJECT DETAILS

In this study, we used mice, primary cells and cell lines as experimental models.

### Mice handling

hCyp3A4 mice were purchased from Taconic (Taconic USA Model #9048). All mice were kept in a SPF facility and experimental procedures have been approved by the Government of upper Bavaria (Regierung von Oberbayern). Male mice have been used for the reported experiments. 6wk old male mice were fed with a chow / high fat diet / low fat diet as indicated (Rodent Diet with 60 kcal% from fat - Research Diet D12492i, Rodent Diet with 10 kcal% from fat – Research Diet D12450B). 5EU (7848.2, Carl Roth) was solubilized in saline 0.9% NaCl. HD5EU was solubilized in a 25% PEG-400, 5% DMSO saline solution. Compounds were administered intraperitoneally at a dose of $0.15_{mg/g}$ 5EU / $0.3_{mg/g}$ HD5EU in a total volume of 200µl. First administration was routinely carried out at Zeitgeber (ZT)3 (9:00 am) so as to avoid circadian effects. For blood and organ collection, mice were terminally anesthetized with Ketamin/Xylazine at indicated times following drug administration. Heart puncture was performed and blood collected in EDTA coated syringes. Blood was centrifuged at 4.8K rpm for 10 minutes followed by 12K rpm for 20 minutes, and then filtered through a 22uM PES filter (PA59.1, Carl Roth). For isolation of primary hepatocytes, 8-10wk old male mice were anesthetized and the liver

was perfused through the vena cava with GIBCO's liver perfusion buffer (17701-038, GIBCO) and liver digestion buffer (17703-034, GIBCO) in accordance with manufacturer's instructions. All other organs were collected and snap frozen in liquid nitrogen and / or fixed in formalin for 48 hours before tissue processing.

### Cell culture

Isolated primary hepatocytes were counted using the countess automated cell counter (C10227, invitrogen), and plated to a density of 75k/cm$^2$ on Geltrex (A1413201, ThermoFisher) coated coverslips (200 μg/cm$^2$) in Williams' Medium E (A12176, GIBCO) supplemented with GIBCO's Primary Hepatocyte Maintenance Supplements (CM4000, GIBCO). 24 hours following plating, cells were treated with 1mM of 5EU (7848.2, Carl Roth) or HD5EU for 8 hours. Azamulin (SML0485, Sigma Aldrich) was added at a concentration of 20 μM for 30 minutes before addition of indicated compounds to a final concentration of 10 μM for the length of the treatment.

## METHOD DETAILS

### Tissue processing and imaging

Tissues were collected and fixed in a neutral buffered 10% formalin solution (HT501128, Sigma) for 48 hours before dehydration and embedding in paraffin. 4 μm sections were cut on a Leica microtome (RM2165, Institute of Experimental Genetics), rehydrated and stained using the Click-iT RNA Alexa Fluor 594 Imaging Kit (C10330, ThermoFisher) in accordance with manufacturer's instructions. Mounting was done with Vectashield hardset antifade mounting medium with DAPI (H-1500, Vector Laboratories). Imagining was done using a Laser Scanning Confocal Microscope (Olympus Fluoview 1200, Institute for Diabetes and Cancer, Neuherberg, Germany) equipped with an Olympus UPlanSApo 60x 1.35 Oil immersion objective.

### Western Blot

Tissues were homogenized using a Miltenyi gentleMACS Dissociator (Miltenyi biotec) in RIPA buffer supplemented with protease (S8820, Sigma Aldrich) and phosphatase (88667, Thermo Fisher) inhibitors. Protein concentration was measured using a standard Bradford assay reagent (B6916, Sigma Aldrich).40μg total protein were loaded per samples on a pre-cast gradient 4%–12% gel (NW04120, Invitrogen). Proteins were transferred to a PVDF membrane (ISEQ00010, Merck Millipore) blocked and blotted using the iBind system (SLF1020, Invitrogen) with primary anti-CYP3A4 (MA5-17064, Thermo Fisher), anti-Phospho-p53 S392 (#9281, cell signaling), anti-total-p53 (#2524, cell signaling), anti-cleaved Caspase-3 (ab214430, abcam), anti-total Caspase-3 (#ab184787, abcam), and anti-HSP90 (SC-7949, Santa-Cruz), and secondary IgG HRP (7076 and 7074, Cell Signaling). Chemiluminescence detection was done using the Pierce ECL Western Blotting Substrate (#32209, Termo Fischer) and images acquired on an iBrightFL1000 (Invitrogen).

### RNA extraction and qRT-PCR

Plasma RNA was extracted using TRI Reagent BD (T3809, Sigma Aldrich), in accordance with manufacturer's instructions. RNA from tissues was extracted using NucleoZOL (740404.200, Macherey-Nagel) reagent, in accordance with manufacturer's instructions. For qRT-PCR, reverse transcription was conducted using the high-Capacity cDNA Reverse Transcription Kit (4368814, Applied Biosystems), in accordance with the manufacturer's instructions. Real-time was carried out on a quant-studio 6 flex (applied biosystems) with SYBR Green PCR Master Mix (#4309155 applied biosystems) and primers; hCyp3-F: TTGGCATGAGGTTTGCTCTC; hCyp3-R: ACAACGGGTTTTTCTGGTTG; Actin-F: CACAGCTTCTTTGCAGCTCCT; Actin-R: CAGCAGTGCAATGTTAAAAGG.

### RNA pull-down and library construction

Pull-down of 5EU labeled RNA was done using the Click-it Nascent RNA Capture Kit (C10365, Thermo Fisher). 10μg total / small RNA was used as input for RNA pull-down from tissues, while 200ng of plasma RNA was used as input for RNA pull-down from blood. Pulled-down RNA was used as the RNA template for library construction using the CATS mRNA/small RNA kit (C05010043 and C05010040, Diagenode) with slight modifications to protocol. These modification include Poly-A selection and RNA fragmentation prior to biotinylation and pull-down of 5EU label RNA using the Click-it Nascent RNA Capture Kit. Following reverse transcription of pulled-down RNA using the CATS kit, cDNA from tissues was amplified for 14 cycles, while plasma RNA was amplified for 20 cycles. As input control 10ng of RNA was used for library construction from tissue / plasma, with an identical number of amplification cycles.

### UPLC-UHR-ToF-MS analysis

For Mass spectrometric analysis, 10μg long / short RNA was used. RNA was digested as described in Sue et al. (2014). Mass spectrometric analysis of nucleotides from RNA was performed on a Waters Acquity UPLC (Waters, Eschborn, Germany) coupled to a Bruker maXis UHR-ToF-MS (Bruker Daltonic, Bremen, Germany). Separation was performed on a Thermo Hypersil Gold column (150 × 1.0 mm, 3 μm, 25003-151030, Thermo Fisher) using a multistep gradient with 100% water and 100% ACN, both with 0.1% formic acid. Gradient conditions were as followed: 0-6 min 0% B, 6-7.65 min linear increase to 1% B, 7.65 to 10 min linear increase to 6% B, 10 to 12 min linear increase to 50% B, 12 to 14 min linear increase to 75% B, 14 to 17 min isocratic hold of 75% B, 17 to 17.5 min return to initial conditions. Column temperature was 36°C and flow rate was set to 0.09 ml/min. Before

each run the column was re-equilibrated for 3 minutes with starting conditions. High mass accuracy was achieved by infusion of 1:4 diluted ESI low concentration tune mix (Agilent Technologies, Waldbronn, Germany) at the start of each chromatographic run. Each analysis was internally recalibrated using the tune mix peak at the beginning of the chromatogram using a custom VB script within Bruker DataAnalysis 4.0 (Bruker Daltonic, Bremen, Germany). Quantitative analysis was performed in Bruker QuantAnalysis 4.0 (Bruker Daltonic, Bremen, Germany). High Resolution-Extracted Ion Chromatograms (HR-EICs) were created around each precursor mass ± 0.005 Da. Chromatograms were smoothed and peak areas were used for quantification. In case of 5EU additional quantification was performed on a validated in-source fragment $[M-132+H]^+$. As standards adenosine (#A921, Sigma-aldrich), guanosine (#G6752, Sigma-aldrich), cytidine (#C4654, Sigma-aldrich) and uridine (#U3750, Sigma-aldrich) were used together with 5EU (7848.2, Carl Roth).

## QUANTIFICATION AND STATISTICAL ANALYSIS

Basic statistical analyses have been performed using GraphPad Prism version 8.3.1, MS Excel and R. Experiments have been performed in biological triplicates (n = 3 animals) and – where possible – in technical duplicates. Results are expressed as mean ± SD. Sequencing experiments have been performed in biological triplicates (n = 3 animals) except for sequencing of plasma samples, which has been performed in biological duplicates (n = 2 animals) with pools of 2 animals/biological sample. Details on the statistical tests used for specific experiments are reported in the main results section.

### Bioinformatic analysis

RNA Libraries were sequenced on an Illumina HiSeq 2500 instrument (**IGA Technology Services Srl, Italy)** at 75bp single-ended. Adaptors were trimmed in accordance with the CATS mRNA/small RNA kit manufacturer's instructions (C05010043 and C05010040, Diagenode) using Cutadapt (Martin, 2011). Trimmed and quality filtered reads were aligned to the mouse mm10 genome using the STAR aligner (Dobin et al., 2013) and a reference transcript GTF file downloaded from Ensembl ((Zerbino et al., 2018), GRCm38.39) which was modified to contain tRNA transcripts as annotated by GtRNAdb (Chan and Lowe, 2016).

For the detection of differentially regulated genes between HFD and LFD the DEseq2 package was used (Love et al., 2014). Pull-down enrichment analysis was conducted using the NOISeq package (Tarazona et al., 2011). Transcripts with expression values smaller than a CPM of 1 and a coefficient of variation greater than 300 were filtered out prior to TMM normalization and enrichment analysis with the NOISeq package. GO and gene set enrichment was calculated using the *Enrichr* tool (Chen et al., 2013).

## DATA AND CODE AVAILABILITY

Raw data for the RNA expression profiles (total, mRNA and smallRNA) have been deposited and are available under the accession code: GSE143562.